

Localization of quantum walk with classical randomness: Comparison between manual methods and supervised machine learning

Christopher Mastandrea¹ and Chih-Chun Chien^{1,*}

¹*Department of Physics, University of California, Merced, CA 95343, USA*

A transition of quantum walk induced by classical randomness changes the probability distribution of the walker from a two-peak structure to a single-peak one when the random parameter exceeds a critical value or the system size exceeds the localization length. We first establish the generality of the localization by showing its emergence in the presence of random rotation or translation. The transition point can be located manually by examining the probability distribution, momentum of inertia, and inverse participation ratio. As a comparison, we implement two supervised machine learning methods, the support vector machine and multi-layer perceptron neural network, with the same data. While both manual and machine-learning methods can identify the transition, the two machine-learning methods tend to underestimate the exponent of the localization length because of the fluctuating probability distribution. Our work illustrates challenges facing machine learning of physical systems with mixed quantum and classical probabilities.

I. INTRODUCTION

While classical random walk finds broad applications in physics, chemistry, biology, finance, and many other places [1–3], the simplest quantum analogue, the quantum walk (QW), exhibits interesting probabilistic behavior due to the underlying wavefunction even if all the operations are deterministic [4]. Recently, there is a trend in studying various quantum walks with classical randomness [5–9], in the sense that the parameter set or geometry of QW is drawn from a classical probability distribution. The resulting probability distribution thus has contributions from both classical and quantum randomness. For example, photons [10], trapped ions [11], superconducting qubits [12], and neutral atoms [13] have been experimentally implemented to demonstrate discrete-time quantum walk with classical randomness in the phase factor or walk step to show a transition from quantum dynamics with multi-peaks in real or momentum space to classical-like dynamics with different structures.

Previous theoretical investigations [9, 14–16], on the other hand, have pointed out the resemblance between the localization transition in quantum walk with classical randomness and the Anderson localization [17], a paradigmatic phenomenon in condensed matter physics. The conventional theory of Anderson localization was first developed within the context of electronic transport, where quantum transport of electrons encounters a localization transition as the parameters from the underlying materials are drawn from a classical probability distribution. Ref. [18] proposed a scaling theory applicable to higher dimensions, from which it can be shown that in one and two dimensions, any amount of disorder will lead to electron localization in the thermodynamic limit. Nevertheless, in a finite system, localization due to classical randomness only occurs when the system size exceeds

the localization length. For example, Ref. [14] evaluates the localization length inferred from the inverse participation ratio. The finite localization length helps explain why quantum walk is experimentally realizable in finite-size systems even if imperfections or fluctuations in the apparatus are unavoidable. Other types of QW, such as Grover QW [19, 20] and QW in inhomogeneous [21, 22] or Floquet-driven systems [23], may also exhibit localization.

Meanwhile, machine learning has become a powerful tool in physics, which has been applied to a broad range of problems like phase transitions [24, 25], dynamics [26], gravitational wave detection [27, 28], searching for new physics [29], etc. More applications are reviewed in Refs. [30–34]. Since the identification of the localization transition of QW with classical randomness is a demanding task when performed manually, we seek help from machine learning to automate the analysis. As a first attempt, we test two elementary supervised machine learning methods, the support vector machine (SVM) and multi-layer perceptron neural network (MLP NN). The two methods have been applied to a variety of problems, such as searching for new universal classifications of classical jammed systems using neural networks [35] and predicting topological properties of materials using SVM [36]. Interestingly, we will show that both methods tend to systematically underestimate the scaling behavior of the localization transition due to the highly oscillatory patterns and continuous transforms of the probability distributions.

To demonstrate the universal behavior of the localization of QW with classical randomness, we introduce three types of classical probabilities, one discrete and the other two continuous, into the rotation and translation operators of the QW. We first use physical quantities, including the patterns of probability distribution, moment of inertia (MoI), and inverse participation ratio (IPR), to manually locate the critical point. We then test the hypothesis that the labor- and time- demanding task of determining

* cchien5@ucmerced.edu

the scaling behavior of the localization length can be handled automatically by supervised machine learning, such as the SVM and MLP NN. We will show that while the SVM and NN can differentiate the localized and delocalized regimes, both methods underestimate the exponent of the localization length from both methods. Therefore, QW with classical randomness provides an example with both quantum and classical probabilities that is challenging to the popular supervised machine learning methods.

The rest of the paper is organized as follows. Sec. II briefly reviews discrete-time quantum walk and introduces three types of classical randomness through the rotation or translation operators. Sec. III presents the localization transition and documents the three manual and two machine-learning methods for analyzing the transition. Sec. IV compares the results from the manual and machine-learning methods and shows the machine-learning methods tend to under-estimate the exponent of the localization length. We also compare the localization to the Anderson localization and discuss implications for experimental or theoretical research. Finally, Sec. V concludes our work.

II. THEORETICAL BACKGROUND

A. Discrete quantum walk

We consider discrete-time QW on a 1D lattice following the description of Ref. [37], beginning with a quantum walker described by a wavefunction defined on a 1D lattice with two internal orthonormal coin states ($|+\rangle, |-\rangle$) on each site. The total state of the walker is taken to be a superposition of the $|+\rangle, |-\rangle$ degrees of freedom, $|\psi\rangle = \sum_x (\alpha_{x,+}|x, +\rangle + \alpha_{x,-}|x, -\rangle)$, where x labels the lattice sites and $\alpha_{x,+} = \langle x, +|\psi\rangle$, $\alpha_{x,-} = \langle x, -|\psi\rangle$ are the complex-valued probability amplitudes for each coin state.

The QW uses two operators, the rotation operator \hat{C} and the translation operator \hat{T} . The translation operator is defined by $\hat{T}|\psi_x, +\rangle = |\psi_{x+1}, +\rangle$ and $\hat{T}|\psi_x, -\rangle = |\psi_{x-1}, -\rangle$. Thus, the translation operator acts to shift the $|+\rangle$ state by one lattice site in the positive direction and the $|-\rangle$ state by one site in the negative direction. The rotation operator is defined as a general unitary operator acting on the coin states at each site and is given by $\hat{C}(\theta, \phi_1, \phi_2) = \begin{pmatrix} \cos(\theta) & e^{i\phi_1} \sin(\theta) \\ e^{i\phi_2} \sin(\theta) & -e^{i(\phi_1+\phi_2)} \cos(\theta) \end{pmatrix}$. The rotation operator mixes the $|+\rangle$ and $|-\rangle$ states at each lattice site, acting as the quantum analog to the coin flip of the classical random walk. Throughout the paper, we will set $\phi_1 = \phi_2 = \frac{\pi}{2}$ so that the coin operator is only dependent on θ , i.e., $\hat{C} = \begin{pmatrix} \cos(\theta) & i \sin(\theta) \\ i \sin(\theta) & \cos(\theta) \end{pmatrix}$. The total state of the walker after some time t is found through repeatedly applying the rotation and translation operators to the walker's initial state. $|\psi(t)\rangle = \hat{T}\hat{C}\hat{T}\hat{C}\cdots\hat{T}\hat{C}|\psi_0\rangle =$

$$(\hat{T}\hat{C})^t|\psi_0\rangle.$$

If the quantum walk only runs up to a time N , the discrete walk may be performed on a $2 \times (N + 1)$ array, where N is the maximum amount of time or steps during a given walk. Here open boundary condition is used since the walker never moves beyond the lattice. We remark that periodic boundary condition may be used but the wavefunction may interfere with itself after it traverses the whole lattice. An extra lattice site to accommodate the initial location is added to the middle of the lattice, so that the lattice has a symmetric amount of steps in both directions. \mathcal{N}_t is defined to be the amount of time allowed for a given walk to evolve through. Hence, $\mathcal{N}_t \leq N$. We consider an initial state with an equal superposition of the $|+\rangle$ and $|-\rangle$ states at the origin, $|\Psi_0\rangle = \frac{1}{\sqrt{2}}(|0, +\rangle + |0, -\rangle)$ and study how the wavefunction spreads out in the lattice.

B. Quantum walk with classical randomness

In addition to the quantum probability from the wavefunction in a quantum walk, we introduce classical randomness that may come from imperfections or fluctuations of the apparatus or environment. There are many ways to add classical randomness to quantum walk. As mentioned, Ref. [14] allows random values of the phase angle ϕ in the rotation operator. Here we introduce three other types of classical randomness that will be analyzed later.

1. Discrete random angles in rotation

We first introduce classical randomness to the quantum walk by using two rotation operators instead of just one. The two rotation operators $\hat{C}_{1,2}$ have their θ values given by $\theta_1 = \theta_0 + \Delta\theta$ and $\theta_2 = \theta_0 - \Delta\theta$ while all the ϕ -angles are set to $\pi/2$. At each step of the walk, we flip a fair classical coin to choose from $\theta_{1,2}$. Explicitly, $P(\theta = \theta_1) = 1/2 = P(\theta = \theta_2)$ at each step. The walk is evolved through the normal application of the chosen coin operator and the translation operator repeatedly. Therefore, the two rotation operators and the translation operator are deterministic, but the classical coin adds an additional probability distribution to the quantum walk. In our simulations, we scan through values of $\Delta\theta$ over the range $0 \leq \Delta\theta \leq \theta_0$ to locate the localization transition.

2. Continuous random angle in rotation

To connect to systems with continuous classical randomness, we consider a quantum walk with random rotation, where the angle θ of the rotation operator is determined by a uniform distribution, in contrast to the binary distribution in the previous case. Explicitly, the angle θ in

each step of one simulation is given by $\theta(t) = \theta_0 + \Delta\theta(t)$, where $\Delta\theta(t)$ is drawn from a uniform distribution between $(0, \Delta\theta_M)$ for a given $\Delta\theta_M$. The ϕ -angles are fixed at $\pi/2$. Next, we scan through different values of $\Delta\theta_M$ by running individual simulations for each value of $\Delta\theta_M$ and obtain the probability distributions from the wavefunction. We remark that Ref. [16] also implements continuous changes of the rotation to study the localization and entanglement between the rotation and translation degrees of freedom of QW.

3. Random translation

We consider another type of classical randomness in quantum walk. In line with the quantum walk operation, there is only one fixed rotation operator throughout the walk. However, an inverse-translation operator is introduced and is defined by $\hat{T}^{-1}|\psi_x, +\rangle = |\psi_{x-1}, +\rangle$ and $\hat{T}^{-1}|\psi_x, -\rangle = |\psi_{x+1}, -\rangle$, such that it reverses the action of the original translation operator, $\hat{T}^{-1}\hat{T}|\psi_x\rangle = |\psi_x\rangle$. We introduce quantum walk with random translation by adding classical probability at every step to choose whether the translation \hat{T} or the inverse translation \hat{T}^{-1} is applied after the rotation operator. A probability P_r is assigned to the inverse translation. Explicitly, $P(\hat{T}^{-1}) = P_r$ and $P(\hat{T}) = 1 - P_r$. If $P_r = 0$, it is the QW without classical randomness while the maximal randomness occurs when $P_r = 0.5$. If $P_r > 0.5$, the result is symmetric with respect to that with $1 - P_r$ because of the parity symmetry between \hat{T} and \hat{T}^{-1} .

III. LOCALIZATION TRANSITION

The classical randomness can be increased by increasing $\Delta\theta$, $\Delta\theta_M$, or P_r in the aforementioned models, and a localization transition starts to emerge. In the following, we discuss how the localization transition can be identified via different methods.

A. Manual methods

1. Final probability distribution

The probability distribution of the walk at a given time can be found by summing over the probabilities on both coin states: $P(x) = \sum_x (|\psi_+(x)|^2 + |\psi_-(x)|^2)$. Selective representatives of the final probability distributions of the cases with discrete random rotation and random translation are shown in Fig. 1. One can see that when the classical randomness is weak, such as small $\Delta\theta$ or P_r , the quantum walker spreads out with two peaks in both directions of the lattice. However, when the classical randomness is strong, the probability distribution concentrates around the initial location with a single-peak

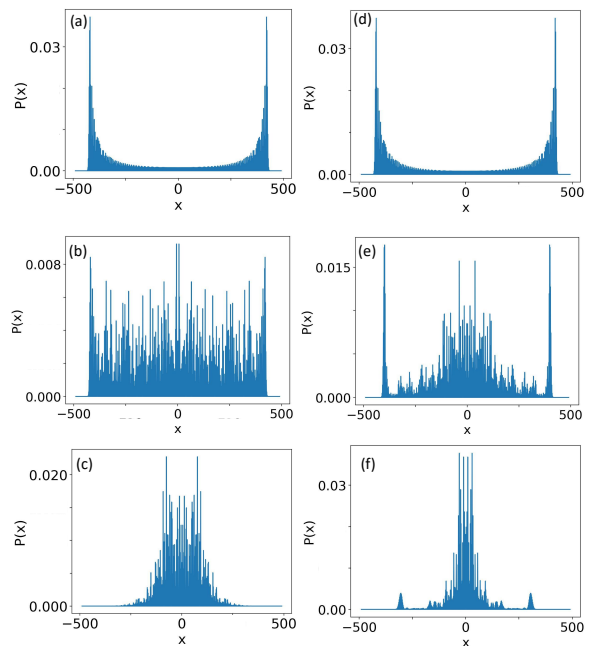


FIG. 1. Localization transition of QW with classical randomness: The probability distributions indicate the system in the delocalized (top row), critical (middle row), and localized (bottom row) regimes as the classical randomness increases. The left column shows the case with discrete random rotation operator with $\theta_0 = \frac{\pi}{6}$, $N = 490$. Panels (a), (b), (c) are at $N_t = 50$, $N_t = 130$, and $N_t = 400$. The right column shows the case with random translation with $\theta_0 = \frac{\pi}{6}$, $N = 490$. Panels (d), (e), (f) are at $P_r = 0.005$, $P_r = 0.045$, and $P_r = 0.15$.

structure, indicating localization of the walker. Therefore, a localization transition occurs at a critical value of the classical randomness. As shown in the middle panels of Fig. 1, the probability distributions may behave differently in the transition regime for different types of classical randomness. For the discrete and continuous random rotations, the probability distribution becomes flat at the transition. However, the case with random translation exhibits a three-peak structure in the transition regime.

By comparing the final probability distributions with a fixed N_t of evolution but different values of classical randomness, the transition region can be found visually by identifying the probability distributions that has a flattened-out pattern or a three-peak structure. Later on, we will see that the three-peak structure of QW with random translation imposes challenges for machine learning.

2. Moment of inertia

Next, we use the idea of moment of inertia (MoI) from classical mechanics as another measure of localization.

The MoI is defined as $MoI(t) = \sum_{x>0} P(x,t)(N-x)^2$, where x labels the position in the lattice, $P(x,t)$ is the probability for the walk to be at x at a given time t , and the maximal run time is assumed to be less than N in the simulation. The inclusion of only $x > 0$ is due to the mirror symmetry about the origin. The MoI is calculated at each step in the evolution after the rotation and translation operators have been applied. For a given $\Delta\theta$, $\Delta\theta_M$, or P_r , we plot the MoI as a function of time. The MoI defined here decreases when the probability distribution spreads away from the origin. The two-peak structure in the delocalized regime thus has less MoI compared to the one-peak localization.

As shown in the top panel of Fig. 2, there is a change of the scaling of the MoI for a fixed set of parameters as time evolves. The critical value of the system size is determined by the time when the scaling behavior changes. On the other hand, the lower panel of Fig. 2 shows that the scaling behavior of the MoI as a function of the classical randomness changes if the simulation time N is fixed and the MoIs of walks with different values of $\Delta\theta$ are plotted. The critical value $\Delta\theta_c$ can be found by locating the "kink" in the MoI curve for both discrete and continuous random-rotation quantum walks. A similar procedure also locates the critical P_c for the quantum walk with random translation, despite the quantitatively different behavior in the transition regime as shown in Fig. 1.

3. Inverse Participation Ratio

The IPR uses higher moments of the wavefunction to reveal the concentration of the distribution. We follow Ref. [14] with the definition

$$IPR = \frac{(\sum_x |\psi_{x,+}|^2)^2}{\sum_x |\psi_{x,+}|^4}. \quad (1)$$

The IPR is maximal if the wavefunction spreads out evenly and decreases if there are spikes in the distribution. Figure 3 shows the IPR as a function of time for a fixed set of parameters and the IPR as a function of the magnitude of classical randomness for a fixed run time N .

The maximum of the IPR indicates the transition point, where the probability distribution is relatively flat. However, one can see that the IPR decreases for smaller or larger $\Delta\theta$. The reason is that the IPR does not discern if the wavefunction has one peak, as in the localized case, or two peaks, as in the delocalized case. Therefore, the IPR cannot differentiate the different phases. However, the coincidence of a relatively flat wavefunction at the transition allows us to use the maximum of the IPR as a quick check for the scaling of the critical behavior. For QW with random translation, the probability distribution in the transition region is still relatively flat compared to the localized or delocalized regimes, despite its

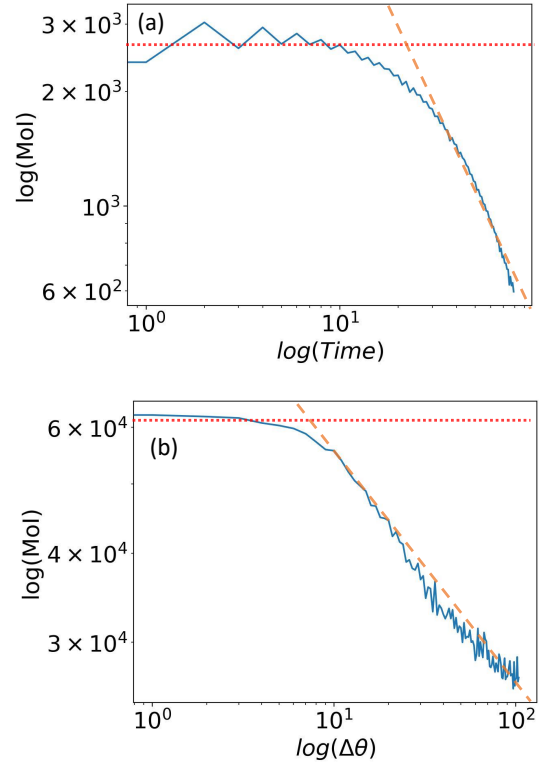


FIG. 2. Moment of Inertia (MoI) of QW with discrete random rotation (a) as a function of time with $\theta_0 = \frac{\pi}{6}$ and $\Delta\theta = 0.04$ and (b) as a function of $\Delta\theta$ with $\theta_0 = \frac{\pi}{6}$ and $N_t = 210$. The solid and dashed lines show the behavior in different regimes.

three-peak structure. Therefore, the IPR still shows a maximum in the transition regime.

B. Supervised machine learning

Despite the success of the aforementioned methods for identifying the localization transition of quantum walk with classical randomness, one usually needs to examine a large number of data sets from the large parameter space for an estimation of the transition region, making the process very demanding on time and resources. Here we investigate the potential for machine learning to automatically identify and differentiate between the delocalization and localization behavior of quantum walk with various classical randomness. Similar to the task of identifying phase transitions in physical systems by machine learning [38, 39], we implement two basic supervised learning methods to find the critical values of the quantum walk with classical randomness. We first feed to the machine the data from weak- and strong- randomness regimes with two different labels, respectively. After the machine can confidently differentiate the two cases according to the labels, we generate data with intermedi-

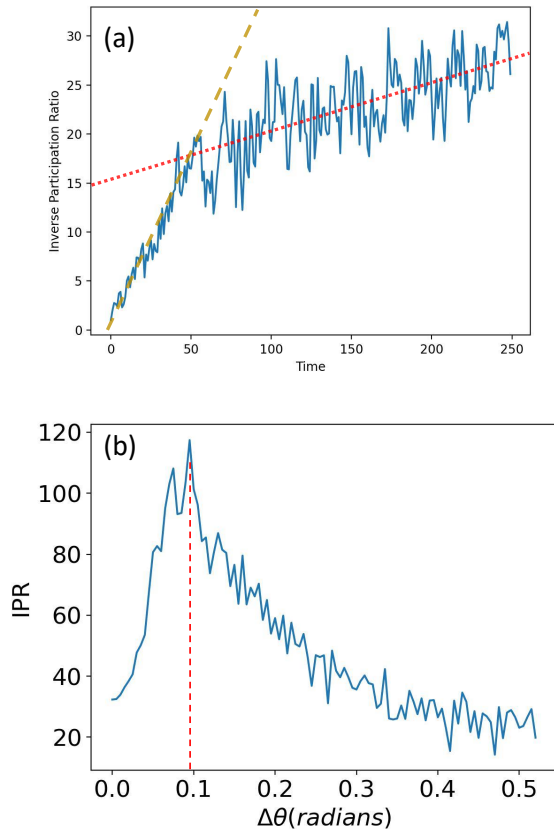


FIG. 3. Inverse participation ratio (IPR) of QW with discrete random rotation (a) as a function of time with $\theta_0 = \frac{\pi}{6}$ and $\Delta\theta = 0.08$. The dashed and dotted lines show the trends on the two sides of the transition and (b) as a function of $\Delta\theta$ with $\theta_0 = \frac{\pi}{6}$ and $\mathcal{N}_t = 250$. The vertical dashed line at the maximum offers an estimation of the transition.

ate randomness and ask the machine for the probabilities of the new data belonging to the two groups. The critical point is determined by the maximal confusion point, where the machine outputs equal probabilities. The two supervised machine learning methods that will be tested are the support vector machine (SVM) and multi-layer perceptron neural network (MLP NN).

1. SVM

We begin with the SVM and train a supervised version from the sklearn linear SGD Classifier on two data sets with the same amount of run time and θ_0 . The first (or second) set of samples is from simulations with a small range of the classical randomness in the delocalized (or localized) regime supplemented with the label "0" (or "1"). The classifier is the "modified hubber" loss function to generate binary classification probabilities instead of the typical "hinge" loss function tailored towards pure true-false binary classification. When training the clas-

sifier, a fraction of the samples from each set were held back to act as a verification set that the trained classifier could correctly distinguish between the two final states. Once the classifier has been trained on the labeled data sets, we preform a test using the reserved samples and checking the classification probabilities to confirm that it is able to distinguish between the delocalization and localization behavior. The small range for generating the training data in the respective regimes with weak and strong randomness is 0.02 for $\Delta\theta$ in the random rotation case and 0.1 for the P_r in the random translation case. We remark that if the range is too small, the data may not give the machine enough information about the configurations. However, if the range is too large, the information of the transition regime may be involved in the data and affect the reliability of the decision of the critical value.

After the training, the data set used to identify the transition region is generated throughout the regime with intermediate randomness. At each $\Delta\theta$ or P_r , the probability distribution is obtained up to the walk length \mathcal{N}_t . Using a classifier trained on a given \mathcal{N}_t , the test data are fed into the classifier. After plotting the probabilities associated with the testing data in the intermediate regime as shown in Fig. 4, the critical value ($\Delta\theta_c$ or $P_{r,c}$) near the transition point is taken to be the maximally confusing point, where the two classification probabilities are equal.

We have also checked the influence of the amount of samples used for training the classifier. To find a minimum sample size we were mainly concerned with the relative stability of the estimates of the critical values from the classifier. As seen in the bottom of Fig. 4, a relatively small training data set is already able to distinguish the overall trend of the localization transition, but the results are more convergent as the total amount of samples used increases. For the localization problem, we found that with a training set of about 2000 samples, the estimates for the critical value already settle into a more stable pattern with few extreme estimates. Increasing the size of the training data further does not lead to visible improvement. In the following, we will present results with a training data set of sample size 1800, as it achieves the minimization of the outlying estimates while being computationally manageable for a large range of $\Delta\theta$, P_r values.

2. Neural networks

Next, we implement a fully connected feed-forward neural network called the multi-layer perceptron neural network (MLP NN) as a supervised learning method to identify the localization transition of QW with classical randomness. We use the network provided by sklearn's MLPClassifier which implements a multi-layer perceptron binary classifier network. In constructing this clas-

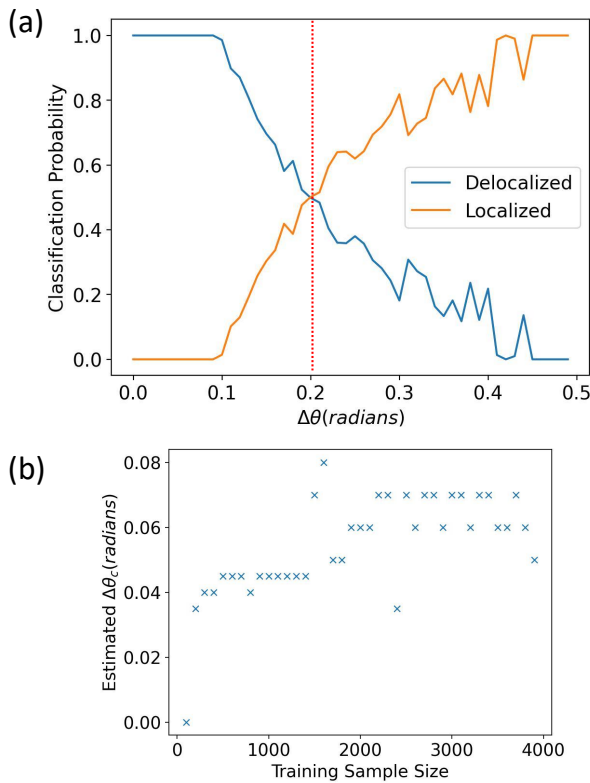


FIG. 4. (a) Training and testing the SVM to classify the localization transition of QW with discrete random rotation. Here $\theta_0 = \frac{\pi}{6}$ and $N = 100$. The vertical dashed line indicates the maximal confusion, which locates the value of $\Delta\theta_c$. (b) Dependence of the critical value determined by the SVM on the size of the training data set.

sifier, we follow the same procedure that was outlined and used with the SVM method. Since we wish to compare with the SVM, we train and employ the NN on the same data sets that were used with the SVM. When training the NN, sklearn’s GridSearchCV library was used to help in working a range of given hyper-parameters to find potential combinations that lead to either greater efficiency in the computational resources needed for convergence, or ones that would lead to greater accuracy in the critical value estimates. Although there is a broad range of hyper-parameter available, we focused on two of the more immediate parameters, the hidden layer sizes and the regularization parameter α .

In our investigation involving the neural network, we used a total of four hidden layers of sizes 400, 200, 100, and 50 to handle the training data with length up to 1000 of each set (corresponding to $N = 500$), as we found this to be a relatively simple “middle ground” that did not add a great amount of computational time while improving the overall estimates. After some trial and error, the regularization parameter was taken to be $\alpha = 0.001$ since this combination of parameters provided reasonable accuracy. While both the SVM and MLP NN methods

take the critical value to be the point of maximal classifier confusion, the NN was found to show a more sudden change in the classification probabilities rather than the more gradual transition found through the SVM. Thus, for the MLP NN, we take the critical value to be the first point where the classification probability of being delocalized falls below 50% as an estimation of the maximally confused point.

3. SVM vs. MLP NN

We estimated the critical values for each of the three types of QW with classical randomness (discrete random angle, continuous random angle, and random translation) using the same training and testing data sets. A comparison between the two learning methods will demonstrate their abilities to generate reliable estimates and more importantly pick up on the scaling trend from the localization transition. Additionally, we investigated the normalization of the data for each method. The probability distribution $P(x)$ of the QW has the default normalization that $\sum_x P(x) = 1$. However, the convention in supervised machine learning is to normalize the distribution so that $P(x)$ spans the range of $[0, 1]$. Therefore, we normalize each probability distribution by its maximal value to ensure $P_{max} = 1$ in each data set to match the normalization that is used within areas like image recognition where machine learning is heavily used. The normalization was performed on both the training and estimation data sets. We found that while the normalization did not improve the estimates given by the SVM, the estimates from the MLP NN did show much less overall variation because neural networks are usually designed with the conventional normalization in mind.

The results shown in Fig. 5 confirm that the two supervised machine learning methods are both capable of classifying the localization transition. Moreover, their estimations of the critical values are fairly similar. On the other hand, both methods appear to produce the same effect in their estimates in that rather than picking out a singular point like the manual methods of the probability distribution, MoI, and IPR, the machine learning programs tend to generate their estimate from a small range around the transition point. Later on, we will see this is likely the cause of the lower scaling exponents of the localization length reported from the machine learning methods.

IV. COMPARISON AND DISCUSSION

A. Comparison of different methods

The localization length sets the limit of the range of the quantum spreading of the wavefunction in the presence of classical randomness. In our simulation, the evolution

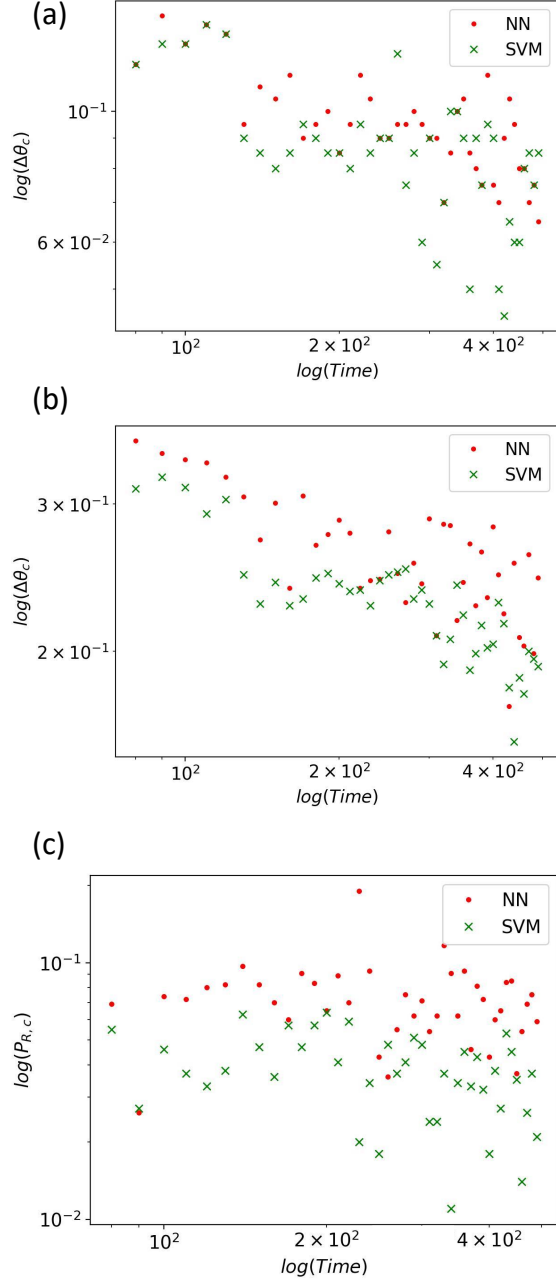


FIG. 5. Critical values of the localization transition from the SVM (crosses) and multi-layer perceptron NN (dots) for QW with (a) discrete random rotation, (b) continuous random rotation, and (c) random translation. All panels are with $\theta_0 = \frac{\pi}{6}$.

time determines the size of the lattice that the quantum walker can explore. To determine the localization length, we first pick a fixed evolution time N and run the simulations for a range of $\Delta\theta$ or $\Delta\theta_M$ for the random-rotation quantum walk or P_r for the random-translation quantum walk. By examining manually the probability distribution, MoI, or IPR, we locate where the localiza-

tion transition occurs and label the critical value $\Delta\theta_c$ or $P_{r,c}$ for the chosen N . Next, we plot the critical $\Delta\theta_c$ or $P_{r,c}$ versus N , as shown in Fig. 6. Viewing the evolution time as a proxy of the system size, Fig. 6 actually reveals the dependence of the magnitude of classical randomness on the length scale. By fitting each set of critical values shown in Fig. 6 with power laws, the exponents associated with the localization length are extracted and summarized in Table I. Moreover, we have checked that the value of $\Delta\theta_c$ is insensitive to the value of θ_0 for the quantum walks with random rotation, as long as θ_0 is away from 0 or multiples of $\pi/2$.

Fig. 6(a) shows the critical values of $\Delta\theta_c$ of QW with discrete random rotation. The three manual methods from the final probability distribution, MoI, and IPR find a similar trend in the critical values. On the log-log scale, all three sets of critical values appear to be nearly parallel, indicating a power-law dependence of the localization length with the randomness magnitude. Meanwhile, the critical values from the SVM are among the critical values from the manual methods, confirming the ability of supervised machine learning to identify the localization transition. However, a closer examination shows that the power-law fit of the SVM results leads to a smaller exponent compared to the three manual methods. The MLP NN produces results close to those from the SVM, so we do not show them to over-crowd the panel. Next, Fig. 6 (b) shows the critical values of $\Delta\theta_c$ from all four methods for QW with continuous random rotation. Despite the difference in the classical distribution (discrete vs. continuous), the similar behavior between Fig. 6 (a) and (b) support the universal scaling behavior of the localization length. We remark that the step-like patterns are due to the limited resolution of the parameters.

Finally, Fig. 6 (c) shows the critical values of $P_{r,c}$ of QW with random translation from manual and machine-learning methods. The similar features indicate the universal scaling of the localization transition. However, there is a much greater amount of variation across all four methods. The MoI particularly shows the most variation. The variation is due to an increase in the fluctuations within the probability distributions of QW with random translation when compared to those from QW with random rotation. Nevertheless, the power-law dependence of the data further supports the universal scaling behavior of the localization transition.

The exponent from the SVM is quantitatively less than those from the manual methods in all three cases. For small values of N_t , the machine-learning methods tend to generate estimates that are slightly into the delocalized regime, possibly due to the challenge to differentiate the two peaks in the probability distribution for small-sized systems. In contrast, they give estimates closer to the localized regimes for larger N_t values, possibly because of the noisy behavior in the probability distribution. While the ML methods still provide fairly accurate estimates of the critical value when compared to the manual meth-

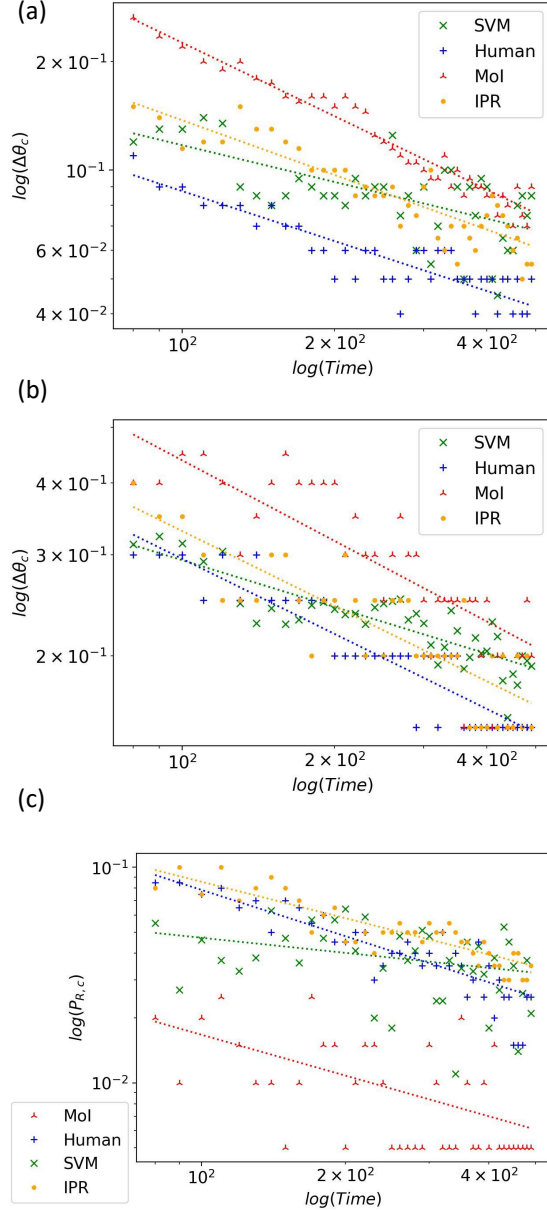


FIG. 6. Comparison of the critical values separating the localized and delocalized regimes estimated from the four methods for QW with (a) discrete random rotation angle, (b) continuous random rotation angle, and (c) random translation direction. The dashed lines show the power-law fit. Here "Human", "MoI", "IPR", and "SVM" correspond to the probability distribution, momentum of inertia, inverse participation ratio, and supervised learning using the SVM, respectively.

ods, the systematic under- and over- estimations flatten out the scaling trend and render the systematically lower scaling exponents compared to the manual methods, as shown in Table I.

Moreover, we found that both SVM and MLP NN show difficulty in estimating the transition region for QW with

	SVM	MLP NN	MoI	Human	IPR
$\Delta\theta_c$ (discrete)	0.366	0.271	0.676	0.460	0.534
$\Delta\theta_c$ (continuous)	0.298	0.258	0.466	0.434	0.434
$P_{r,c}$	0.149	-0.050	0.628	0.712	0.561

TABLE I. Exponents of the power-law dependence of the critical value on the size of the walk. The "Human" method is from the manual determination of the final probability distributions.

random translation. As shown in Fig. 1, the transition regime of QW with random translation is complicated due to the coexistence of the central peak and the two side peaks. In an effort to dissuade the machine from systematically under- or over- estimating the transition points, we split the probability distributions up into three regions: (1) $-N < x < -N/2$, (2) $-N/2 < x < N/2$, and (3) $N/2 < x < N$. Regions (1) and (3) contain the left- and right-most peaks seen in panel (e) of Fig. 1 while region (2) contained the neighborhood of the origin showing the evolution from a flat, delocalized distribution to the localized central peak. The three regions were then separately used as the new training data sets to generate the new transition region estimates. Using these sets of disseminated data for the SVM and MLP NN, we found no observable improvements in the transition estimates using either of these regions. The results also help us see that the two machine-learning methods weight in both local and global features of the data rather than catching some prominent variations. For the SVM method, there seems to be little potential for improvement or loss of information over using the entire probability distributions compared to these smaller regions. With the MLP NN however, this lack of improvement further highlights the difficulty that the commonly available machine-learning method faces when attempting to differentiate systems that have mixed quantum and classical probabilities.

B. Connection to Anderson localization

The Anderson localization [17] is usually described by the random hopping model on a lattice with the Hamiltonian

$$H_A = \sum_{\langle i,j \rangle} t_{ij} c_i^\dagger c_j + H.c. + \sum_j V_j c_j^\dagger c_j. \quad (2)$$

Here c_j^\dagger (c_j) is the creation (annihilation) operator on site j , t_{ij} is the hopping coefficient between the nearest-neighbor pair $\langle i, j \rangle$, and V_j is the onsite potential. The classical randomness of the hopping model can be introduced by drawing t_{ij} or V_j from uniform distributions within the range $(0, W)$ in each step. One may view the random rotation (or translation) of QW as the analogues of the random onsite potential (or hopping) of the Anderson model. While the 1D and 2D ground states in the thermodynamic limit are localized according to the Anderson model [40], there can be delocalized states in

3D above a threshold energy.

Ref. [41] provides a functional form for the 1D localization length of the Anderson model. A relation between the localization length L_{loc} and the amplitude of the disorder W is written in the form $L_{loc} \propto W^{-2} \Rightarrow W \propto L_{loc}^{-0.5}$. Their experimental results support this scaling behavior. In our results of quantum walk with classical randomness, we have identified a similar localization transition. The exponents shown in Table I suggest universal behavior and a deep connection with the Anderson localization. While there are different ways of introducing classical randomness via the rotation or translation operator with discrete or continuous distributions, the exponents from all the manual methods seem to be around 1/2, the value suggested by the Anderson localization. In contrast, the two machine learning methods seem to under-estimate the exponent, as explained in the previous subsection. We remark that Ref. [24] has shown machine learning can differentiate the phases across the Anderson localization in a quasi-periodic lattice, where the deterministic parameters induces the transition, in contrast to the cases we consider here that mix quantum and classical probabilities.

C. Implications

Our analysis of QW with classical randomness has shown the universal behavior of the localization transition, which transcends different methods for inducing classical randomness. Realizations and measurements of quantum walk with classical randomness have been achieved. For example, Ref. [13] used atomic Bose-Einstein Condensate (BEC) to experimentally implement a discrete-time QW. Classical randomness called "noise" has been introduced through the phase factor of the coin operator, resulting in a change of the momentum distribution associated with the transition from quantum to classical walk dynamics. In Ref. [11], a single ion in a linear Paul trap allows for the control of its internal states through a series of controlled $\frac{\pi}{2}$ pulses. Like Refs. [13, 14], they introduce classical randomness through the coin phase parameter, using a random noise generator for each of the pulses, and show the change from the quadratic propagation speed of QW to the linear speed of a classical random walk. In Ref. [10], an all-optical implementation of a discrete-time QW using entangled pairs of photons that were split at each step but with one being directly used in the walk while the other acting as a trigger for the measurements. The internal states were the left-handed and right-handed polarization states. By differing the angle of the mirrors in each step, the photons can decohere. Over a small number of walk steps ($N_t = 6$), the probability distributions are shown for QW and for the decohered walk with Gaussian-like structure and lin-

ear propagation speed associated with a classical random walk.

The under-estimate of the exponent of the localization length from the two supervised machine learning methods provides an example that mixing classical and quantum probabilities is still a challenging task for basic machine learning methods. While we can manually resort to physical quantities such as the MoI or IPR to pinpoint the critical point, the machine associates certain features with the labels for classification. We have seen the classification may be constrained by limitation of the data size or distraction from the fluctuating part in the bulk of the data. Our results thus present an open challenge for machine learning to better differentiate systems with both classical and quantum probabilities.

In our investigations with neural-network based classification, we had focused on using the MLP classifier as it provides a plain and immediate interface to various problems. While this classifier is able to generate classification predictions of a certain level of accuracy, it may show a tendency to overfit the predictions [42–44] and thus bias the final results. A potential improvement on this is the convolutional neural network based classifier [45–47]. This type of neural network, while requiring more work to correctly tune its relevant hyper-parameters, has shown improvement over the MLP classifier in the overall accuracy of estimations and reduced potential for overfitting when used on more complex data sets [48–50]. The localization transition of QW with classical randomness is expected to serve as a suitable problem for testing and benchmarking machine learning methods.

V. CONCLUSION

The resemblance between the localization transition of QW with classical randomness and the Anderson localization helps us explore the localization length via different ways of introducing classical randomness to establish its universality. While the localization transition realizable in many experiments can be characterized manually by physical quantities such as the MoI or IPR, the supervised learning methods using the SVM and MLP NN catch the transition but under-estimate the exponent of the localization length. The deviation is particularly significant in QW with random translation, given its more structured probability distribution in the transition regime. Our results will inspire future research on systems with mixed quantum and classical probabilities and applications of machine learning to those systems.

ACKNOWLEDGMENTS

We thank David Colby for some early explorations of the problem.

-
- [1] T. Aquino and M. Dentz, Phys. Rev. Lett. **119**, 230601 (2017), URL <https://link.aps.org/doi/10.1103/PhysRevLett.119.230601>.
- [2] K. Chipman and A. Singh, BMC Bioinformatics **10** (2009), URL <https://bmcbioinformatics.biomedcentral.com/articles/10.1186/1471-2105-10-17>.
- [3] E. A. Codling, M. J. Plank, and S. Benhamou, Journal of the Royal Society, Interface **5**, 813 (2008), URL <https://royalsocietypublishing.org/doi/10.1098/rsif.2008.0014>.
- [4] D. Koch and M. Hillery, Phys. Rev. A **97**, 012308 (2018), URL <https://link.aps.org/doi/10.1103/PhysRevA.97.012308>.
- [5] Y. Yin, D. E. Katsanos, and S. N. Evangelou, Phys. Rev. A **77**, 022302 (2008), URL <https://link.aps.org/doi/10.1103/PhysRevA.77.022302>.
- [6] C. M. Chandrashekar, Phys. Rev. A **83**, 022320 (2011), URL <https://link.aps.org/doi/10.1103/PhysRevA.83.022320>.
- [7] A. Schreiber, K. N. Cassemiro, V. Potoček, A. Gábris, I. Jex, and C. Silberhorn, Phys. Rev. Lett. **106**, 180403 (2011), URL <https://link.aps.org/doi/10.1103/PhysRevLett.106.180403>.
- [8] A. Crespi, R. Osellame, R. Ramponi, V. Giovannetti, R. Fazio, L. Sansoni, F. De Nicola, F. Sciarrino, and P. Mataloni, Nature Photonics **7**, 322 (2013), URL <https://www.nature.com/articles/nphoton.2013.26>.
- [9] T. Rakovszky and J. K. Asboth, Phys. Rev. A **92**, 052311 (2015), URL <https://link.aps.org/doi/10.1103/PhysRevA.92.052311>.
- [10] M. A. Broome, A. Fedrizzi, B. P. Lanyon, I. Kassal, A. Aspuru-Guzik, and A. G. White, Phys. Rev. Lett. **104**, 153602 (2010), URL <https://link.aps.org/doi/10.1103/PhysRevLett.104.153602>.
- [11] F. Zähringer, G. Kirchmair, R. Gerritsma, E. Solano, R. Blatt, and C. F. Roos, Phys. Rev. Lett. **104**, 100503 (2010), URL <https://link.aps.org/doi/10.1103/PhysRevLett.104.100503>.
- [12] J. Ghosh, Phys. Rev. A **89**, 022309 (2014), URL <https://link.aps.org/doi/10.1103/PhysRevA.89.022309>.
- [13] S. Dadras, A. Gresch, C. Groiseau, S. Wimberger, and G. S. Summy, Phys. Rev. Lett. **121**, 070402 (2018), URL <https://link.aps.org/doi/10.1103/PhysRevLett.121.070402>.
- [14] S. Derevyanko, Sci. Rep. **8**, 1795 (2018), URL <https://doi.org/10.1038/s41598-017-18498-1>.
- [15] R. Duda, M. N. Ivaki, I. Sahlber, K. Poyhonen, and T. Ojanen (2022), URL <https://arxiv.org/abs/2210.05310>.
- [16] L. H. Yao and S. Wald (2023), arXiv: 23030.15978.
- [17] P. W. Anderson, Phys. Rev. **109**, 1492 (1958), URL <https://link.aps.org/doi/10.1103/PhysRev.109.1492>.
- [18] E. Abrahams, P. W. Anderson, D. C. Licciardello, and T. V. Ramakrishnan, Phys. Rev. Lett. **42**, 673 (1979), URL <https://link.aps.org/doi/10.1103/PhysRevLett.42.673>.
- [19] N. Inui, Y. Konishi, and N. Konno, Phys. Rev. A **69**, 052323 (2004), URL <https://link.aps.org/doi/10.1103/PhysRevA.69.052323>.
- [20] M. Zeng and E. H. Yong, Scientific Reports **7**, 12024 (2017), URL <https://doi.org/10.1038/s41598-017-12077-0>.
- [21] Y. Shikano and H. Katsura, Phys. Rev. E **82**, 031122 (2010), URL <https://link.aps.org/doi/10.1103/PhysRevE.82.031122>.
- [22] A. Wojcik, T. Luczak, P. Kurzynski, A. Grudka, T. Gdala, and M. Bednarska-Bzdega, Phys. Rev. A **85**, 012329 (2012), URL <https://link.aps.org/doi/10.1103/PhysRevA.85.012329>.
- [23] I. Vakulchyk, M. V. Fistul, P. Qin, and S. Flach, Phys. Rev. B **96**, 144204 (2017), URL <https://link.aps.org/doi/10.1103/PhysRevB.96.144204>.
- [24] J. Carrasquilla and R. G. Melko, Nat. Phys. **13**, 431 (2017), ISSN 1745-2481, URL <https://doi.org/10.1038/nphys4035>.
- [25] Y. Che, C. Gneiting, T. Liu, and F. Nori, Phys. Rev. B **102**, 134213 (2020), URL <https://link.aps.org/doi/10.1103/PhysRevB.102.134213>.
- [26] J. Timoshenko, A. Anspoks, A. Cintins, A. Kuzmin, J. Purans, and A. I. Frenkel, Phys. Rev. Lett. **120**, 225502 (2018), URL <https://link.aps.org/doi/10.1103/PhysRevLett.120.225502>.
- [27] M. B. Schäfer, F. Ohme, and A. H. Nitz, Phys. Rev. D **102**, 063015 (2020), URL <https://link.aps.org/doi/10.1103/PhysRevD.102.063015>.
- [28] V. Boudart and M. Fays, Phys. Rev. D **105**, 083007 (2022), URL <https://link.aps.org/doi/10.1103/PhysRevD.105.083007>.
- [29] G. Karagiorgi, G. Kasieczka, S. Kravitz, B. Nachman, and D. Shih, Nature Reviews Physics **4**, 399 (2022), URL <https://doi.org/10.1038/s42254-022-00455-1>.
- [30] A. Tanaka, A. Tomiya, and K. Hashimoto, *Deep Learning and Physics* (Springer Nature Singapore, Singapore, 2019).
- [31] G. Carleo, I. Cirac, K. Cranmer, L. Daudet, M. Schuld, N. Tishby, L. Vogt-Maranto, and L. Zdeborová, Rev. Mod. Phys. **91**, 045002 (2019), URL <https://link.aps.org/doi/10.1103/RevModPhys.91.045002>.
- [32] P. Mehta, M. Bukov, C.-H. Wang, A. G. Day, C. Richardson, C. K. Fisher, and D. J. Schwab, Physics Reports **810**, 1 (2019), ISSN 0370-1573, a high-bias, low-variance introduction to Machine Learning for physicists, URL <https://www.sciencedirect.com/science/article/pii/S0370157319300766>.
- [33] G. E. Karniadakis, I. G. Kevrekidis, L. Lu, P. Perdikaris, S. Wang, and L. Yang, Nature Reviews Physics **3**, 422 (2021), ISSN 2522-5820, URL <https://doi.org/10.1038/s42254-021-00314-5>.
- [34] E. Bedolla, L. C. Padierna, , and R. Castaneda-Priego, J. Phys.: Condens. Matter **33**, 053001 (2021).
- [35] S. Franz, S. Hwang, and P. Urbani, Phys. Rev. Lett. **123**, 160602 (2019), URL <https://link.aps.org/doi/10.1103/PhysRevLett.123.160602>.
- [36] N. Claussen, B. A. Bernevig, and N. Regnault, Phys. Rev. B **101**, 245117 (2020), URL <https://link.aps.org/doi/10.1103/PhysRevB.101.245117>.
- [37] J. Wang and K. Manouchehri, *Physical Implementations of Quantum Walks* (Springer Nature, New York, London, 2014).

- [38] A. Canabarro, F. F. Fanchini, A. L. Malvezzi, R. Pereira, and R. Chaves, *Phys. Rev. B* **100**, 045129 (2019), URL <https://link.aps.org/doi/10.1103/PhysRevB.100.045129>.
- [39] C.-H. Song, Q.-C. Gao, X.-Y. Hou, X. Wang, Z. Zhou, Y. He, H. Guo, and C.-C. Chien, *Phys. Rev. Res.* **4**, 023005 (2022), URL <https://link.aps.org/doi/10.1103/PhysRevResearch.4.023005>.
- [40] A. Isihara, *Condensed Matter Physics* (Dover Books, Mineola, New York, 1991).
- [41] J. Billy, V. Josse, Z. Zuo, A. Bernard, B. Hambrecht, P. Lugan, D. Clément, L. Sanchez-Palencia, P. Bouyer, and A. Aspect, *Nature* **453**, 891 (2008), URL <https://doi.org/10.1038/nature07000>.
- [42] S. Lawrence and C. L. Giles, in *Proceedings of the IEEE-INNS-ENNS International Joint Conference on Neural Networks. IJCNN 2000. Neural Computing: New Challenges and Perspectives for the New Millennium* (2000), vol. 1, pp. 114–119 vol.1.
- [43] S. Lawrence, C. L. Giles, and A. C. Tsoi, in *Proceedings of the National Conference on Artificial Intelligence* (1997), pp. 540–545.
- [44] D. H. Mantzaris, G. C. Anastassopoulos, and D. K. Lymberopoulos, in *2008 8th IEEE International Conference on BioInformatics and BioEngineering* (2008), pp. 1–6.
- [45] A. Botalb, M. Moinuddin, U. M. Al-Saggaf, and S. S. A. Ali, in *2018 International Conference on Intelligent and Advanced System (ICIAS)* (2018), pp. 1–5.
- [46] S. Lawrence, C. L. Giles, A. C. Tsoi, and A. D. Back, *IEEE Transactions on Neural Networks* **8**, 98 (1997).
- [47] S. B. Driss, M. Soua, R. Kachouri, and M. Akil, in *Real-Time Image and Video Processing 2017*, edited by N. Kehtarnavaz and M. F. Carlsohn, International Society for Optics and Photonics (SPIE, 2017), vol. 10223, p. 1022306, URL <https://doi.org/10.1117/12.2262589>.
- [48] V.-E. Neagoe, A.-D. Ciotec, and G.-S. Cucu, in *2018 International Conference on Communications (COMM)* (2018), pp. 201–206.
- [49] D. C. Cireşan, U. Meier, J. Masci, L. M. Gambardella, and J. Schmidhuber, in *Proceedings of the Twenty-Second International Joint Conference on Artificial Intelligence - Volume Volume Two* (AAAI Press, 2011), IJCAI'11, p. 1237–1242, ISBN 9781577355144.
- [50] S. R. Park and J. W. Lee, in *Proc. Interspeech 2017* (2017), pp. 1993–1997.